

Supplemental Information for

Single-cell Spatial Immune Landscape of ASFV-Infected Porcine Lung Microenvironment

Hui Guo^{1,2,¶}, Huaiyuan Cai^{1,2,¶}, Yu Chen^{1,3}, Zhong Zou², Shengjie Yin^{1,2}, Yangyang Xu^{1,2}, Guiqing Peng^{1,2},
Meilin Jin^{1,2}, Gang Cao^{1,2,4}, Jinxia Dai^{1,2,*}

* Correspondence: Jinxia Dai,

Email: jxdai@mail.hzau.edu.cn

This PDF file includes:

Supplemental Materials and Methods

Figures S1 to S9 with legends

Legends for Table S1

Supplemental Materials and Methods

Infection. Two infection groups (3 piglets/group) were orally challenged with ASFV SY-1 strain (2×10^2 HAD₅₀) using a syringe, and two control groups (3 piglets/group) received an equal volume of solvent. All challenged piglets were monitored daily for rectal temperature until tissue collection. Oral, nasal, and rectal swab samples from the challenged pigs were used to measure the viral load via real-time quantitative PCR (RT-qPCR) of *B646L* gene. The primers for *B646L* gene amplification were ASF-05-Zsak-1466F: 5'-CCTCGGCGAGCGCTTTATCAC-3', ASF-05-Zsak-1528R: 5'-GGAAACTCATTACCAAATCCTT-3', and ASF-05-Zsak-1486prob: 5'-FAM-CGATGCAAGCTTTAT-MGB-3'.

Tissue slice preparation. Pig lung tissues from all lobes (right upper, right middle, right lower, right accessory, left upper, and left lower lobes) and spleen tissues were dissected out, and rinsed in diethyl pyrocarbonate treated PBS (DEPC-PBS) to wash off blood from the surface. Next, tissues were fixed in 4% paraformaldehyde (PFA) in PBS for 24 hours (h) at 4°C. After fixation, tissues were trimmed into $0.5 \times 0.5 \times 0.5$ cm³ blocks and dehydrated in gradient ethanol (75% ethanol for 30 minutes (min), 85% ethanol for 30 min, 95% ethanol for 30 min, 100% ethanol for 20 min once and 10 min twice) followed by double immersion in xylene (15 min + 10 min) and triple immersion in Surgipath Paraplast Plus (Leica Biosystems, 39602004) for 30 min each using an automatic benchtop tissue processor (Leica Biosystems, TP1020). Subsequently, tissue blocks were embedded in paraffin using paraffin embedding machine (Leica Biosystems, EG1150H), then cut into 4 µm sections using automatic rotary slicer (Leica Biosystems, RM2255). Sections were carefully flattened out in DEPC water at 42°C and adhered onto microscope slides, followed by dry overnight at 37°C. All slices were stored at 4°C.

Hematoxylin-Eosin Staining. Hematoxylin-Eosin staining kit (Solarbio, G1120) was used for the staining of tissue slices of pig lungs. Slices were followed by xylene dewaxing (twice, 10 min each), rehydration with graded ethanol (100%, 95%, 85%, and 75% ethanol for 5 min each), and two washes with distilled water for 2 min each. Subsequently, slices were immersed in hematoxylin staining solution for 5 min and rinsed with distilled water for 3 min, followed by differentiation solution treatment for 32 seconds (s) and rinse with distilled water for 1 min. Then slices were immersed in 0.1% ammonia for 25 s and rinsed in distilled water for 5 min. Next, slices were immersed in 80% ethanol for 3 min and then eosin staining solution for 58 s.

Further, slices were treated with 95% ethanol for 35 s, 100% ethanol three times for 3 min each, and xylene twice for 5 min each. Finally, slices were sealed with neutral balsam mounting medium and imaged with Panoramic Scan II digital scanner (3DHISTECH, Hungary).

***In situ* multi-gene mRNA co-detection.** Paraffin slices were subjected to a series of pretreatments including dewaxing (baked in oven at 60°C for 10 min and twice soak in xylene for 10 min each), rehydration (in gradient ethanol of 100%, 95%, 85%, 70%, 50% and 30% for 5 min each), and dehydration (in DEPC-PBS for 5 min). Then, slices were sealed with SecureSeal™ hybridization chambers (Grace, 621505). The slices were treated with proteinase K (2 µg/mL in PBS) at 37 °C for 30 min, followed by one wash with 0.2% glycine for 2 min and triple washes with DEPC-PBSTR (0.1% Tween-20, 0.1 U/µL recombinant RNase inhibitor (RRI) in DEPC-PBS) for 5 min each. Further, slices were fixed with 4% PFA for 10 min and washed three times with DEPC-PBSTR. Finally, slices were dehydrated in a series of 30%, 50%, 70%, 85%, 95% and 100% ethanol for 1 min each, then washed three times with DEPC-PBSTR. Subsequently, slices were subjected to *in situ* multi-gene mRNA co-detection including six steps: annealing of dual-barcode padlock probes and initiator primer probes to cellular mRNA targets, ligation of padlock probes, rolling-circle amplification, detection probes hybridization, imaging, and decoding. Before co-detection, the dual-barcode padlock probes were phosphorylated at the 5' end with T4 polynucleotide kinase (Vazyme, N102-01), then annealed with equal molar (100 µM) of initiator primer probes through cooling down from 95°C to 25°C at a rate of 0.1 °C/s via thermocycler.

The dual-barcode padlock probes (30 nM per probe) with initiator primer probes (30 nM per probe) in hybridization buffer (2X SSC (Sangon, B548109) with 10% formamide (Sangon, A100606), 20 mM ribonucleoside-vanadyl complexes (Beyotime, R0108) and 0.1mg/mL salmon sperm DNA (Thermofisher, AM9680)) were added to the hybridization chamber of slices and incubated at 37°C overnight. Then slices were washed twice with DEPC-PBSTR for 10 min each and once with 4× SSC buffer in DEPC-PBSTR. Next, the ligase reaction buffer (1 U/µL SplintR Ligase (NEB, M0375L), 1× buffer, 0.2 U/µL RRI, and 0.20 µg/µL BSA) was added for 2 h incubation at 25°C. Following ligation, slices were washed with DEPC-PBSTR twice for 5 min each, and incubated with rolling-circle amplification reaction buffer (1 U/µL Phi29 (Vazyme, N106-01), 1× RCA buffer, 0.25 µM dNTP, 0.2 µg/µL BSA, 5% glycerol) at 30°C for 6 h. After triple washes with DEPC-PBSTR for 10 min each, slices were eliminated autofluorescence using TrueVIEW

Autofluorescence Quenching Kit (Vector Labs, SP-8400-15). Finally, the fluorescent detection probes (100 nM per probe) in DEPC-PBST were added to the chamber and incubated for 1 h at 37°C. After triple washes with PBST (PBS with 0.1% Tween-20) for 5 min each, slices were counter stained with DAPI and then immersed in 50% glycerol in PBS for imaging with a Leica TCS SP8 confocal microscope (60× water microscope, NA 1.2). Channels for DAPI, Alexa Fluor 488, Alexa Fluor 546, Alexa Fluor 594, and Alexa Fluor 647 were scanned. LAS X (v.3.7.2.22383; Leica) software was used to acquire images. After each round of imaging, signals were stripped with 60% formamide in 2× SSC at 45°C for 10 min. Then next round of detection was performed by adding the corresponding detection probes.

Spatial autocorrelation analysis. To evaluate spatial autocorrelation of cell distributions, we calculated Moran's I index, which measures clustering or dispersion of a phenomenon in space. The calculation formula

is as follows: $I = \frac{n}{\sum_{i=1}^n \sum_{j=1}^n w_{ij}} \cdot \frac{\sum_{i=1}^n \sum_{j=1}^n w_{ij} (x_i - \bar{x})(x_j - \bar{x})}{\sum_{i=1}^n (x_i - \bar{x})^2}$. Firstly, cell coordinates were extracted from cell masks and used to construct a spatial grid. A kernel density estimate (KDE) of the cell distribution was computed, representing the cell density at each grid point. To quantify spatial relationships, a distance matrix between all grid points was constructed. A spatial weight matrix was defined based on a threshold distance, assigning weights to grid points within this distance. The weight matrix was row-normalized to ensure comparability.

Then global Moran's I statistic was calculated using the density values and the weight matrix. This involved computing the mean density and the deviations from this mean. The numerator was obtained by summing the product of the weighted differences from the mean density for all pairs of points, while the denominator was the sum of the squared differences from the mean density. Moran's I was then derived to assess the degree of spatial clustering or dispersion among the cells. Codes are available at <https://github.com/wikk-chy/Spatialspots>.

Viral-load state determination. We employed the Kneed function to identify two inflection points (9 signal counts and 27 signal counts) in the distribution of cells expressing *B646L* by analyzing the relationship between the signal counts of *B646L* mRNA and the log2-transformed cell numbers. The Kneed function was utilized with different sensitivity parameters (S=6 and S=0.1) to detect the inflection points, or "knees," in

the curve. These inflection points were used to partition infected cells into three viral-load states (Semi, High, and High+). Cells with signal counts of 0 were labeled as 'Bystander'.

Apoptosis analysis of cell type. The TUNEL images were processed to a single channel and smoothed using a Gaussian filter with a sigma of 1 to reduce noise. An Otsu threshold was applied to convert the images to a binary format, allowing for clear differentiation of apoptotic cells. For each cell (represented by its center coordinates from the cell segmentation results), we determined its apoptotic status by checking if the center coordinates had a corresponding value in the binary image.

Wasserstein metric. The Wasserstein metric, also known as the Wasserstein distance, is a measure of the distance between two probability distributions in a metric space. We utilized the KernelDensity function from sklearn.neighbors to compute the probability density distributions of all genes expression. Subsequently, we employed the wasserstein_distance function from scipy.stats to measure the distance between the spatial expression distributions of host and viral genes. Codes are available at <https://github.com/wikk-chy/Spatialspots>.

Spatial immune microenvironment analysis. Data points were divided into regions using K-means clustering (KMeans from sklearn). For each cluster, Kernel Density Estimation (KDE) was performed to identify areas with high gene density. Top density points were identified based on KDE results and further filtered using DBSCAN clustering (DBSCAN from sklearn) to ensure a minimum distance between density centers. Representative points were chosen as the mean coordinates of DBSCAN clusters. KDE results and top density centers were visualized using matplotlib. Based on the field of view and imaging results, three radii were defined: 60 pixels (inner), 120 pixels (middle), and 180 pixels (outer), with $1\ \mu\text{m} = 14.4299\ \text{pixel}$. Distances between center cells and surrounding cells were calculated using Euclidean distance. Cell type counts within these radii were analyzed to understand the distribution of cell types around density centers. Gene expression statistics were computed within specified radii around each density center. The number of cells expressing specific genes was calculated for each radius. To balance area differences among the three regions, gene expression densities were calculated using weights of 15, 5, and 3 for the 60 pixels (inner), 120 pixels (middle), and 180 pixels (outer) regions, respectively. Codes are available at <https://github.com/wikk-chy/SpatialImmunoCircle>.

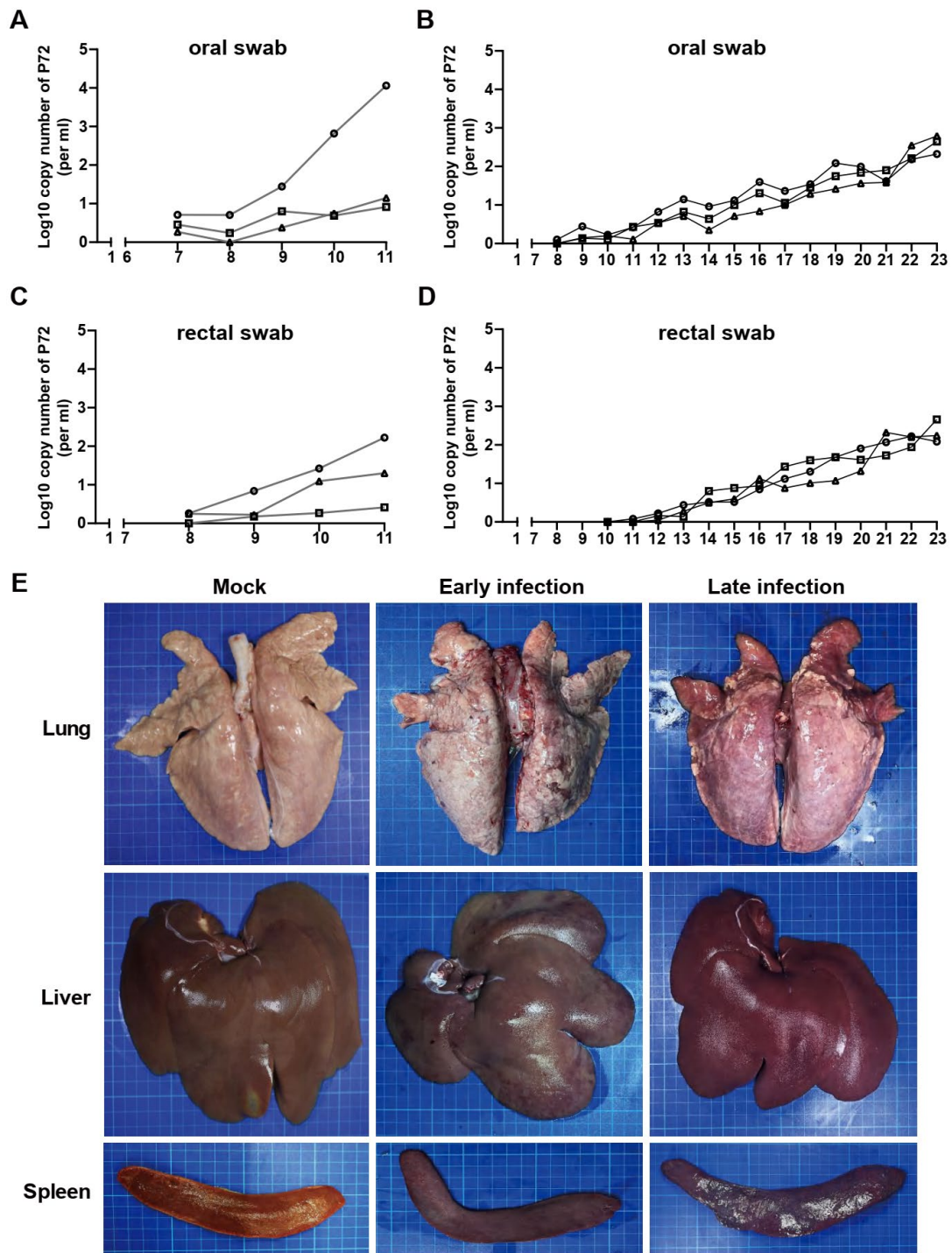


Fig. S1. Viral load and tissue lesion upon ASFV infection

(A-B) Viral copy numbers detected in oral swabs. (C-D) Viral copy numbers detected in rectal swabs. (E)

Gross lesion in lung, liver, and spleen of pigs along ASFV infection.

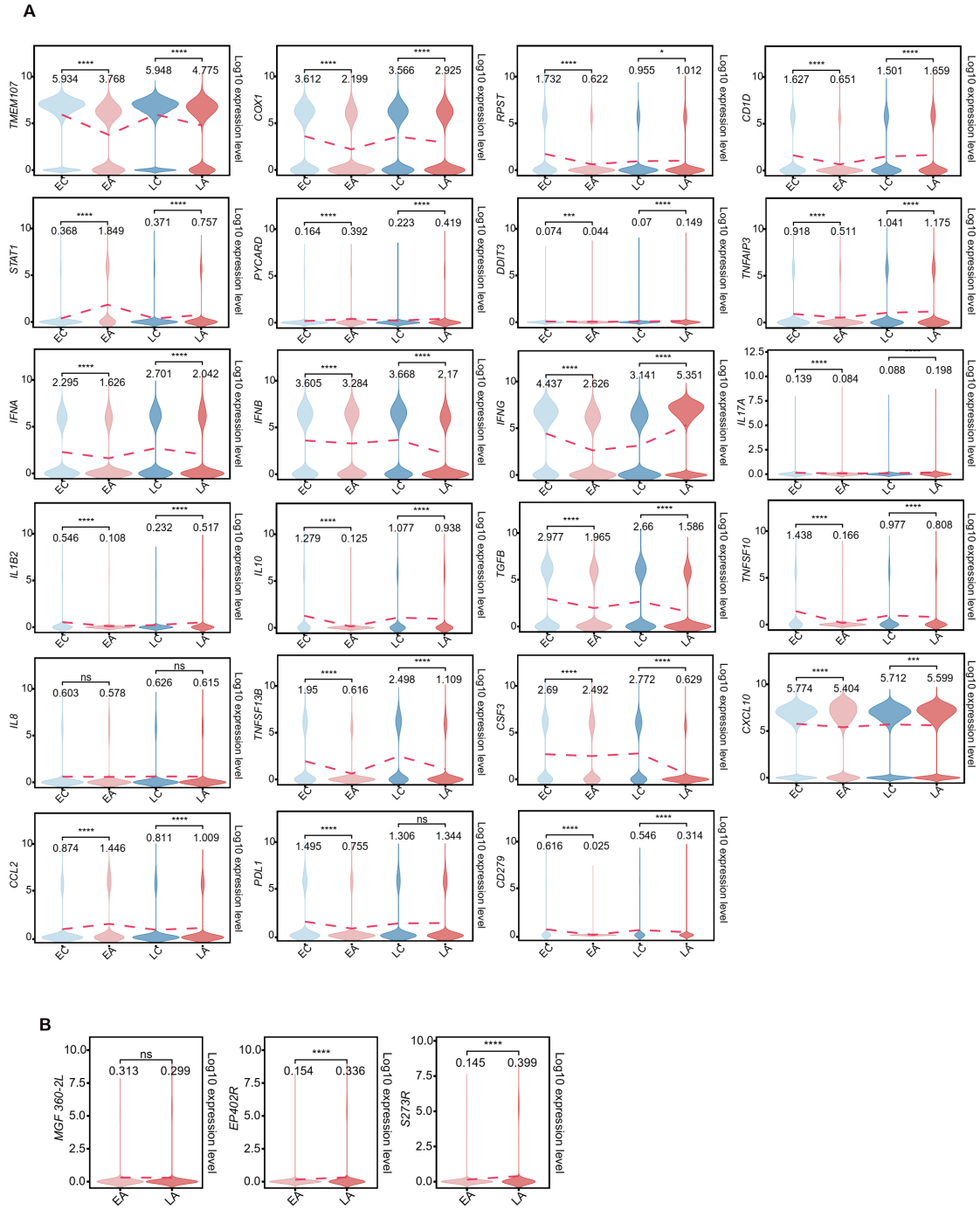


Fig. S2. Violin plots of gene expression change

(A) Violin plots of host genes expression level in host cells of pig lung tissue slices. (B) Violin plots of viral genes expression level in host cells of pig lung tissue slices. Statistical significance was assessed through Wilcoxon rank-sum test. The numbers in the figure represent the median. ns: $P > 0.05$, $*P < 0.05$, $***P < 0.001$.

0.0001. EC, early samples of mock controls; LC, late samples of mock controls; EA, early samples of ASFV infection; LA, late samples of ASFV infection.

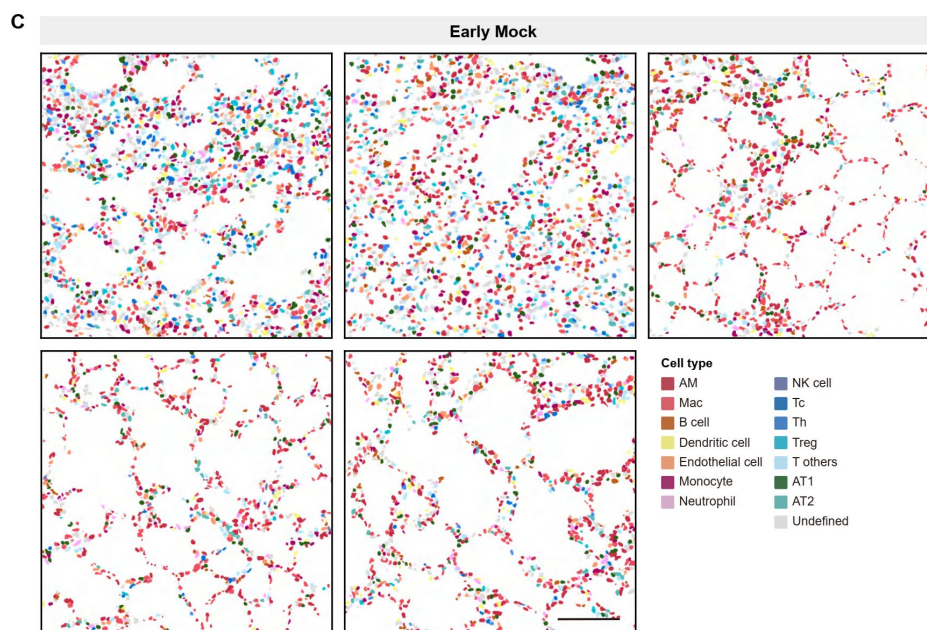
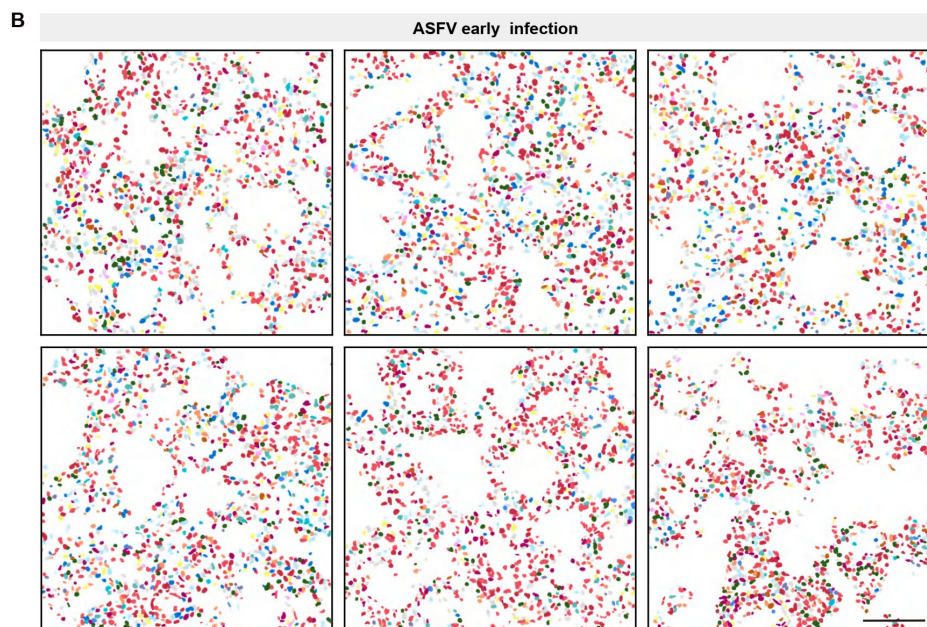
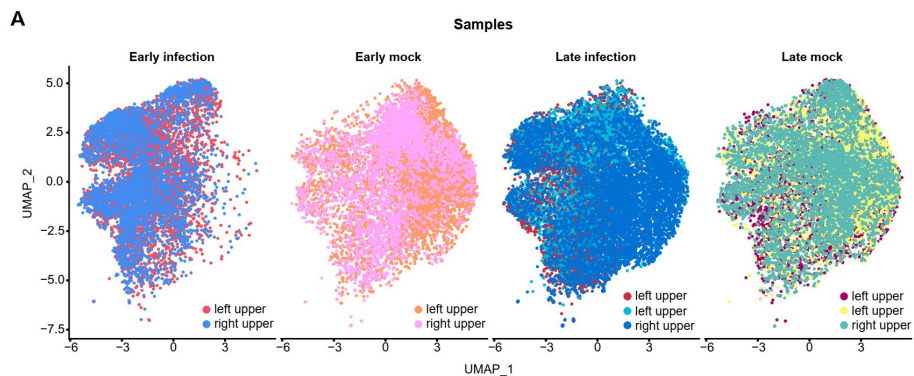


Fig. S3. Images of annotated cell types in slices from early samples

(A) Uniform manifold approximation and projection (UMAP) plot of cell clusters. Distinct colors indicate slices of different pig lung lobes selected for *in situ* mRNA co-detection. (B-C) The remaining images of annotated cells in slices from early infection (B) and control (C) samples. The color representation is same for B and C. Scale bars, 100 μm in B and C.

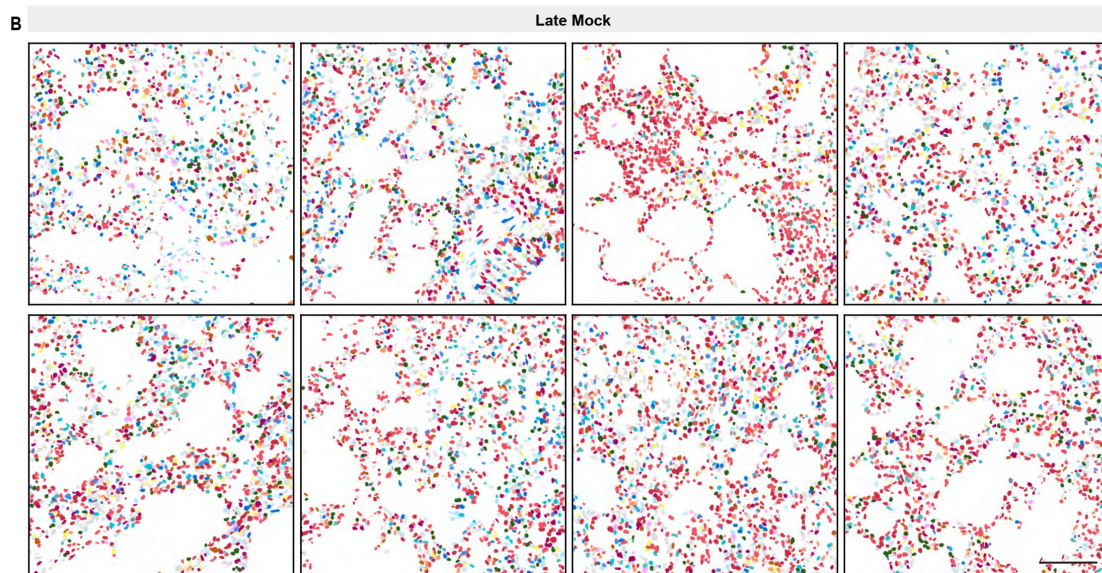
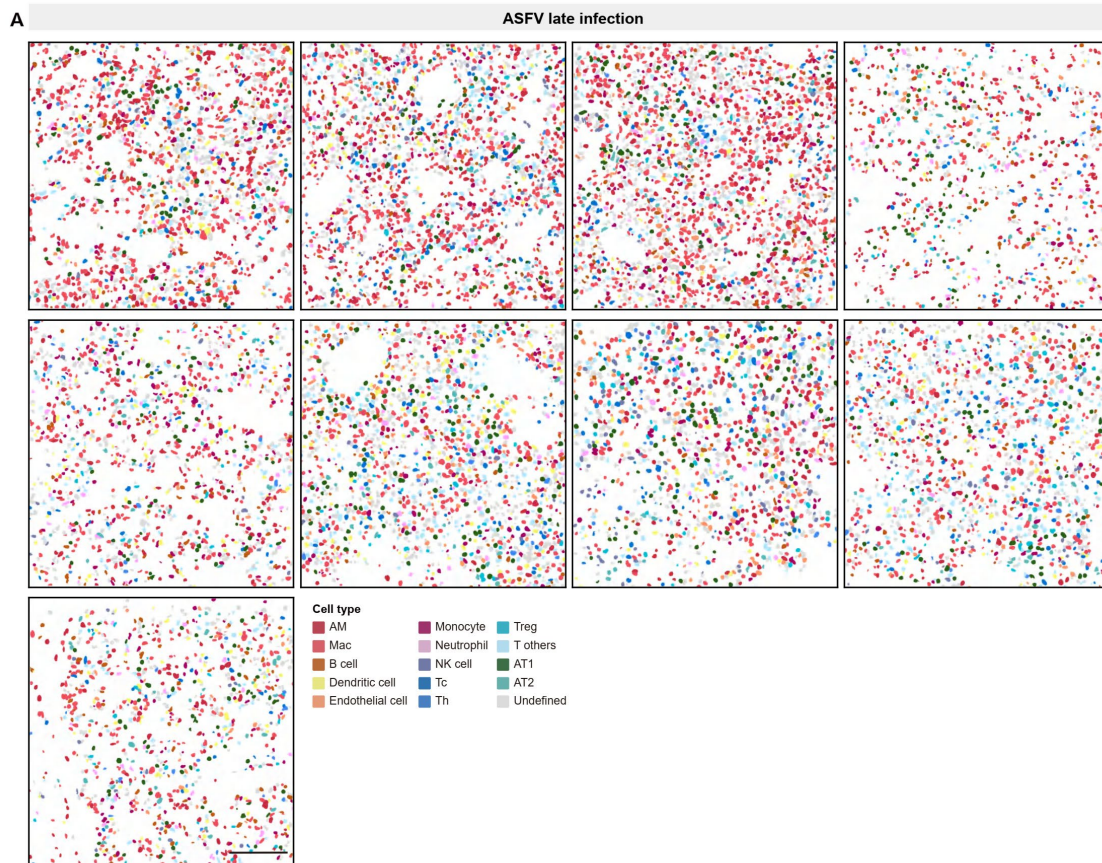


Fig. S4. Images of annotated cell types in slices from late samples

(A-B) The remaining images of annotated cells in slices from late infection (A) and control (B) samples. The color representation is same for A and B. Scale bars, 100 μm in A and B.

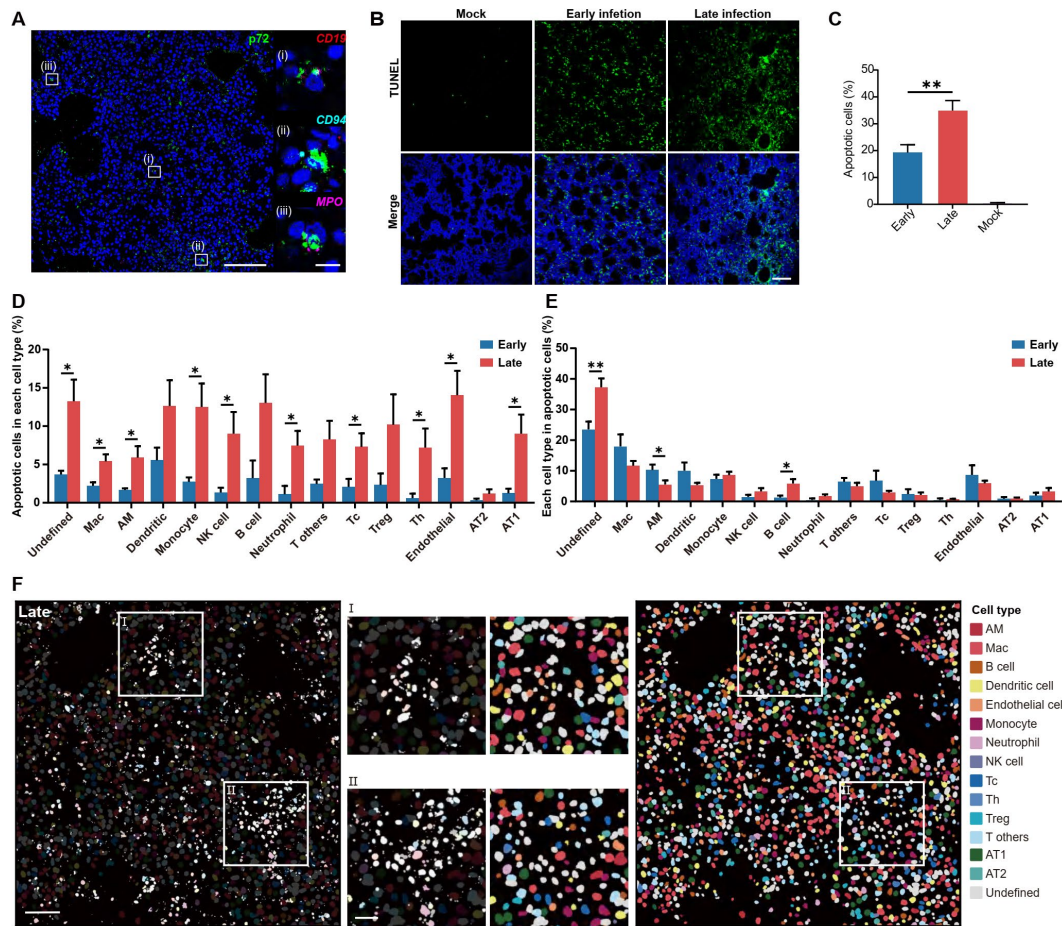


Fig. S5. ASFV infection induces apoptosis in multiple cell types of pig lungs

(A) Co-detection of ASFV P72 and marker genes mRNA of B cells (*CD19*), NK cells (*CD94*), and neutrophils (*MPO*). (B) TUNEL staining images for early and late samples. (C) Significance difference for the proportion of apoptotic cells in early and late samples. (D) Comparison of the percentage for apoptotic cells in each cell type between early and late infection. (E) Comparison for the percentage of each cell type among total apoptotic cells between early and late infection. (F) Images for apoptotic cells in annotated cell types of late infection samples. The bright signal on the left image indicates apoptotic cells overlaid on the dimmed image of colored cell types; the right panel shows the colored cell types in the same image. White boxes areas in lower images were magnified in the middle panel. Sample sizes for C-E: n=6 images for early mock; n=7 images for early ASFV infection; n=9 images for late mock; n=10 image for late ASFV infection. Data was presented as mean \pm SEM for C-E, and statistical significance was determined using Student's t-

test (two-tailed). * $P < 0.05$, ** $P < 0.01$. Scale bars, 100 μm in lower magnification and 10 μm in higher magnification in A, 100 μm in B, 50 μm in lower magnification images and 20 μm in higher magnification images of E.

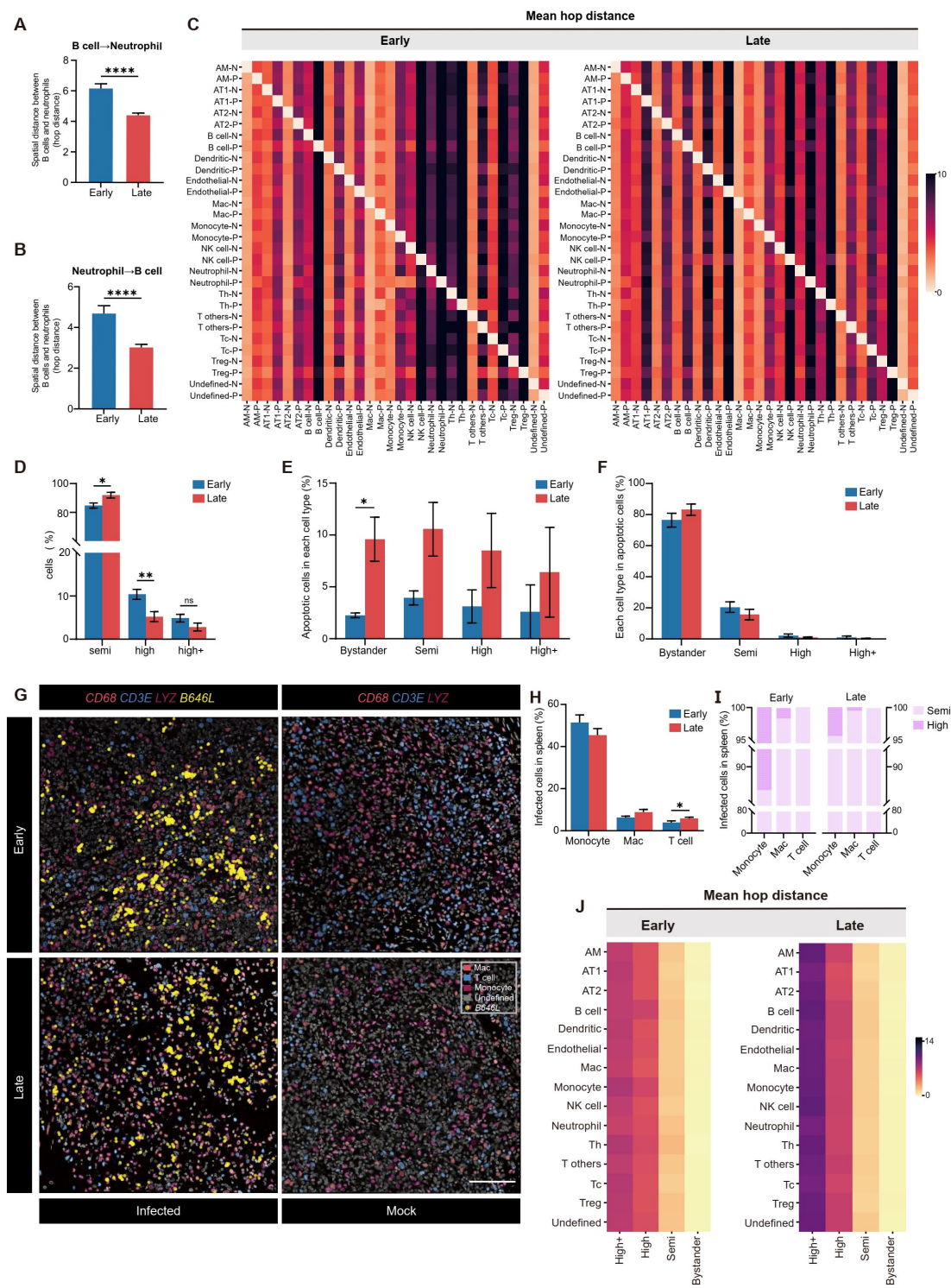


Fig. S6. Changes of cell distribution in pig lung tissue slices upon ASFV infection

(A-B) Change of spatial distance between B cells and neutrophils from early to late stage of infection. (C) Heat map of mean hop distance among different types of cells subdivided into infected and uninfected cells. AT1, alveolar type I; AT2, alveolar type II; AM, alveolar macrophages; Mac, macrophage; NK, natural killer; Tc, cytotoxic T cell; Th, helper T cell; Treg, regulatory T cells. P for positive means ASFV infection, and N for negative means bystander cells. (D) Comparison of cell proportion for three viral-load states in total infected cells between early and late stages of infection. (E) The proportion of apoptotic cells for three viral-load states and bystanders. (F) The cell proportion of three viral-load states and bystanders among total apoptotic cells. (G) *In situ* mRNA co-detection of *CD68* (marker gene for macrophages), *LYZ* (marker gene for monocytes), *CD3E* (marker gene for T cells), and viral *B646L* in slices of pig spleens. Scale bar, 100 μ m. (H) The proportion of ASFV infected cells among monocytes, macrophages, and T cells in spleen samples. (I) The proportion of semi-infected (0-9 counts of *B646L* mRNA signal) and high-infected (signal counts >9) cells in macrophages, monocytes, and T cells of spleen samples. (J) Heatmap of mean hop distance between cells of different viral-load states and 15 types of cells. Sample sizes for A-F: n=6 images for early mock; n=7 images for early ASFV infection; n=9 images for late mock; n=10 image for late ASFV infection. Sample sizes for H-I: n=6 images for early ASFV infection; n=9 images for late ASFV infection. Data was presented as mean \pm SEM, and the statistical significance was measured by Student's t-test (two-tailed). ns: $P > 0.05$, * $P < 0.05$, ** $P < 0.01$, **** $P < 0.0001$.

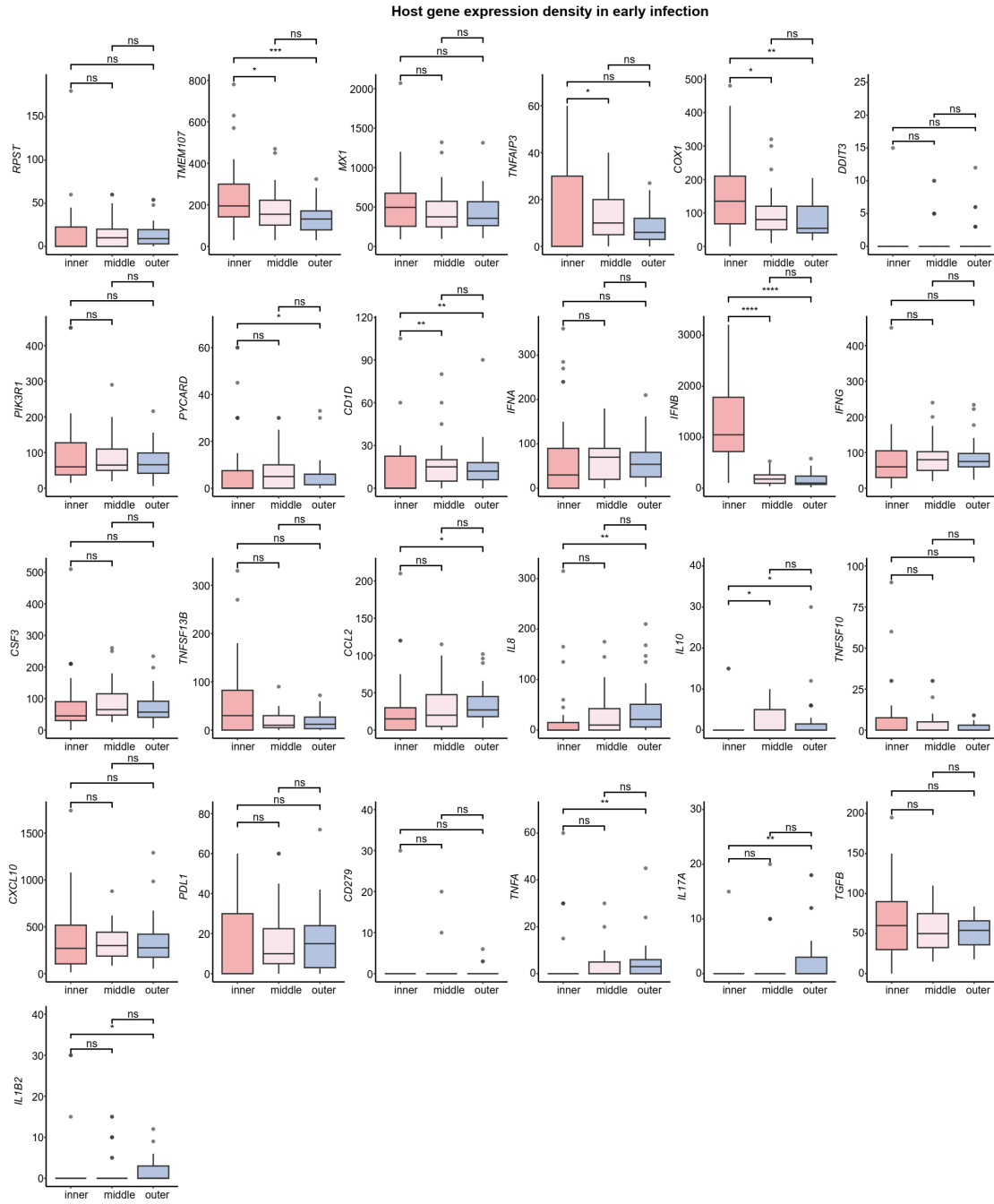


Fig. S7. Box-plots of gene expression around high-infection center at early infection stage

Box-plots of host genes expression density in three layers around high-infection center at early infection stage. Statistical significance was assessed through Wilcoxon rank-sum test. ns: $P > 0.05$, * $P < 0.05$, ** $P < 0.01$, *** $P < 0.001$, **** $P < 0.0001$.

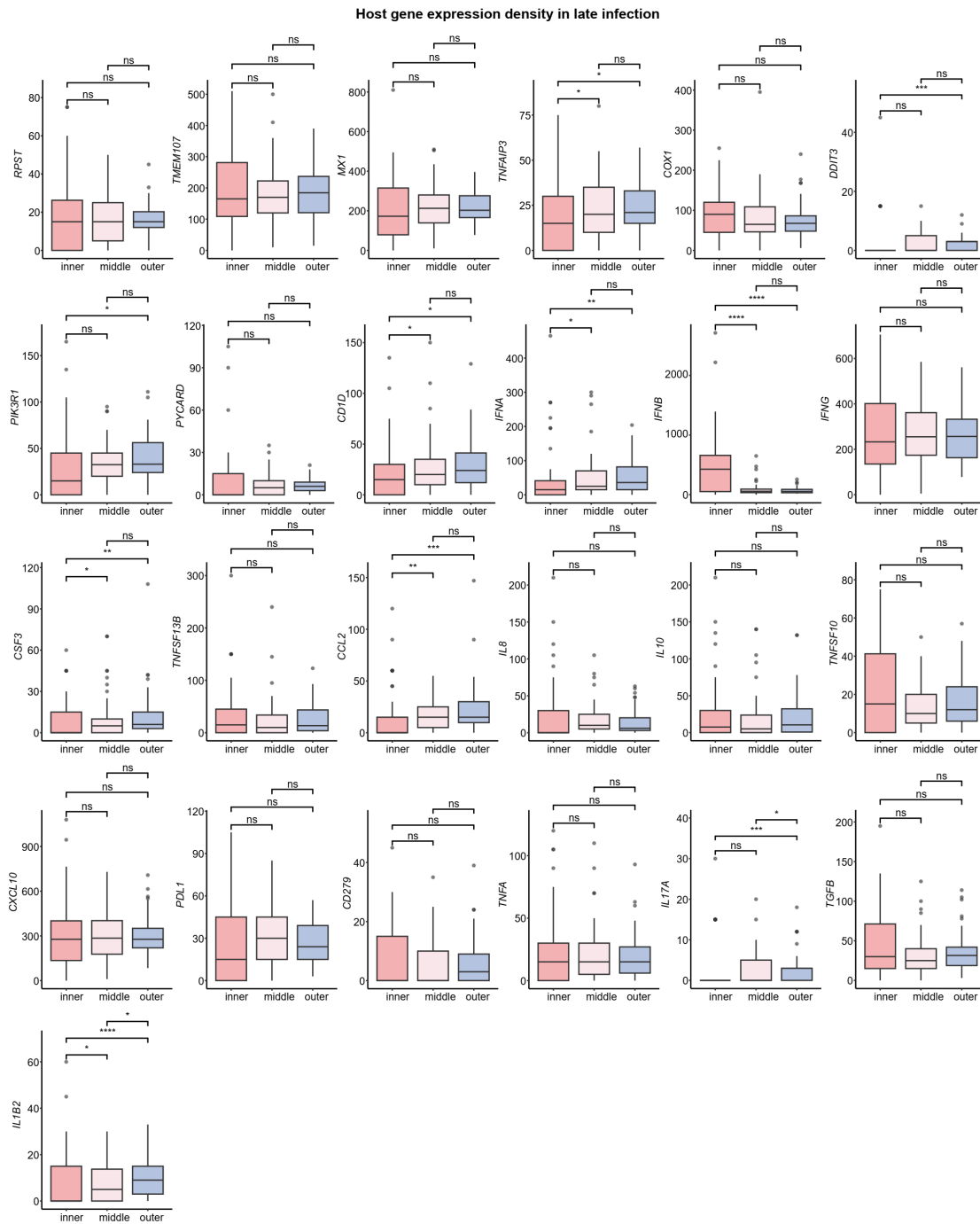


Fig. S8. Box-plots of gene expression around high-infection center at late infection stage

Box-plots of host genes expression density in three layers around high-infection center at late infection stage.

Statistical significance was assessed through Wilcoxon rank-sum test. ns: $P > 0.05$, * $P < 0.05$, ** $P < 0.01$,

*** $P < 0.001$ **** $P < 0.0001$.

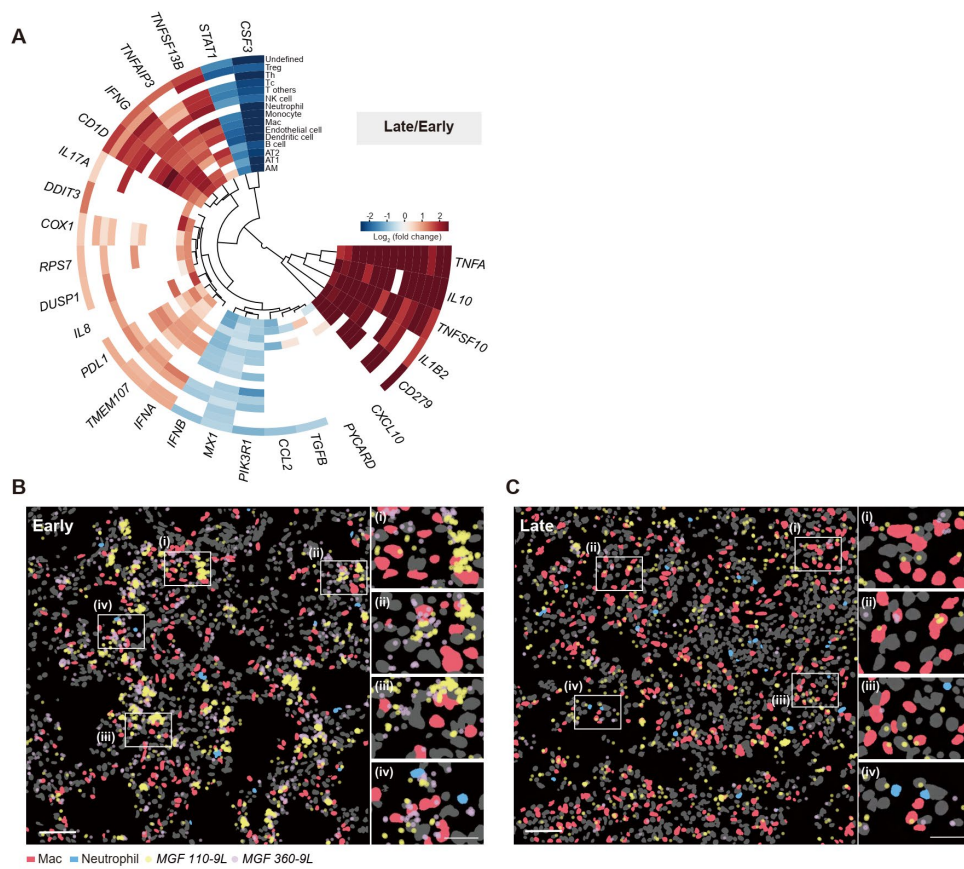


Fig. S9. Host gene expression dynamics in different cell types

(A) Expression change heatmap of 27 host genes in 15 cell types for late infection stage over early infection stage. Red indicates up-regulation, and blue indicates down-regulation. (B-C) Expression of MGF 360-9L and MGF 110-9L in macrophages and neutrophils at early (B) and late (C) infection. The box areas of i-iv are magnified on the right panels. Scale bars, 50 μ m in left panels, 20 μ m in right panels.

Legends for Table S1. Genes list and probe sequences

The genes list (43 host genes and 7 ASFV genes) and the probe sequences for multi-gene in situ mRNA codetection were listed separately.